

Journal of Photonics for Energy

PhotonicsforEnergy.SPIEDigitalLibrary.org

Design and fabrication of cascaded dichromate gelatin holographic filters for spectrum-splitting PV systems

Yuechen Wu
Benjamin Chrysler
Raymond K. Kostuk

SPIE.

Yuechen Wu, Benjamin Chrysler, Raymond K. Kostuk, "Design and fabrication of cascaded dichromate gelatin holographic filters for spectrum-splitting PV systems," *J. Photon. Energy* **8**(1), 017001 (2018), doi: 10.1117/1.JPE.8.017001.

Design and fabrication of cascaded dichromate gelatin holographic filters for spectrum-splitting PV systems

Yuechen Wu,^{a,*} Benjamin Chrysler,^b and Raymond K. Kostuk^{a,b}

^aThe University of Arizona, Department of Electrical and Computer Engineering,
Tucson, Arizona, United States

^bThe University of Arizona, College of Optical Sciences, Tucson, Arizona, United States

Abstract. The technique of designing, optimizing, and fabricating broadband volume transmission holograms using dichromate gelatin (DCG) is summarized for solar spectrum-splitting applications. The spectrum-splitting photovoltaic (PV) system uses a series of single-bandgap PV cells that have different spectral conversion efficiency properties to more fully utilize the solar spectrum. In such a system, one or more high-performance optical filters are usually required to split the solar spectrum and efficiently send them to the corresponding PV cells. An ideal spectral filter should have a rectangular shape with sharp transition wavelengths. A methodology of designing and modeling a transmission DCG hologram using coupled wave analysis for different PV bandgap combinations is described. To achieve a broad diffraction bandwidth and sharp cutoff wavelength, a cascaded structure of multiple thick holograms is described. A search algorithm is then developed to optimize both single- and two-layer cascaded holographic spectrum-splitting elements for the best bandgap combinations of two- and three-junction spectrum-splitting photovoltaic (SSPV) systems illuminated under the AM1.5 solar spectrum. The power conversion efficiencies of the optimized systems are found to be 42.56% and 48.41%, respectively, using the detailed balance method, and show an improvement compared with a tandem multijunction system. A fabrication method for cascaded DCG holographic filters is also described and used to prototype the optimized filter for the three-junction SSPV system. © 2018 Society of Photo-Optical Instrumentation Engineers (SPIE) [DOI: 10.1117/1.JPE.8.017001]

Keywords: solar energy; spectrum splitting; multijunction PV; holography; dichromate gelatin fabrication.

Paper 17119P received Nov. 12, 2017; accepted for publication Dec. 15, 2017; published online Jan. 8, 2018.

1 Introduction

To make better use of the power available in the solar spectrum, photovoltaic (PV) cells with several energy bandgaps are required.^{1,2} This approach allows the efficiency to exceed the detailed balance limit for single bandgap systems of 33%.³ Two approaches to multijunction photovoltaic (MJPV) system design have been developed. In the most common method, a broadband concentrator (BBC) is used to collect light and focus it onto the surface of a tandem MJPV cell. This method allows for high optical efficiencies (>85%) and power conversion efficiencies in excess of 45%. However, the fabrication of tandem MJPV cells is a complex process that requires the growth of energy bandgap materials on top of one another. This requires precise lattice matching between layers and also restricts the range of bandgap energies that can be used. In addition, the current output of the complete cell is limited by the lowest output junction and requires current matching schemes for efficient operation. As a result, tandem MJPV cells are expensive to fabricate, and therefore must be used with high concentration ratio optical collectors to limit the size of the cell.⁴ However, this in turn restricts the field of view of the collector and requires direct sunlight and high accuracy tracking for optimal performance.

*Address all correspondence to: Yuechen Wu, E-mail: ywu2@email.arizona.edu

An alternative approach to BBC-MJPV cell systems is spectrum-splitting collectors (SSC) with a set of single-junction PV cells that have different energy bandgaps.⁵⁻¹⁰ In this approach, the optical system spatially separates incident solar illumination into different spectral bands and directs each band to a PV cell that has the highest response to the spectral band. Since each PV cell is separated, lattice matching is not an issue and different material types can be used.¹¹ In addition, the cells are connected in parallel and the total current is not current limited by the lowest output cell.¹² However, the complexity of the system now resides in the optics, which must effectively separate the different spectral bands of the incident solar illumination and direct them to corresponding cells. The optics must also perform a certain level of concentration at the PV cell surface.¹³

In this paper, a methodology of designing and modeling transmission dichromate gelatin (DCG) holograms for a dispersive spectrum-splitting concentrating PV system using coupled wave analysis is described. To achieve a broad spectral bandwidth with sharp cutoff wavelengths, a cascaded structure of multiple thick holograms is evaluated and compared with single-layer holographic spectrum-splitting elements. A search algorithm is also developed to optimize both single-layer and cascaded two-layer holographic spectrum-splitting elements for the best match with two- and three-junction spectrum-splitting photovoltaic (SSPV) systems illuminated with AM1.5 solar spectrum. A detailed balance analysis method is then used to determine the maximum limit of power conversion efficiency under AM1.5 solar illuminations for the two- and three-junction dispersed SSCPV system. In addition, the optimized two-layer cascaded holographic filter optimized for the three-junction SSPV systems is fabricated using DCG and tested in our laboratory.

2 Evaluating Spectrum-Splitting System

Spectrum-splitting optics must spatially separate different spectral bands of incident solar illumination and direct each band to a specific PV cell. This allows dissimilar PV materials to be

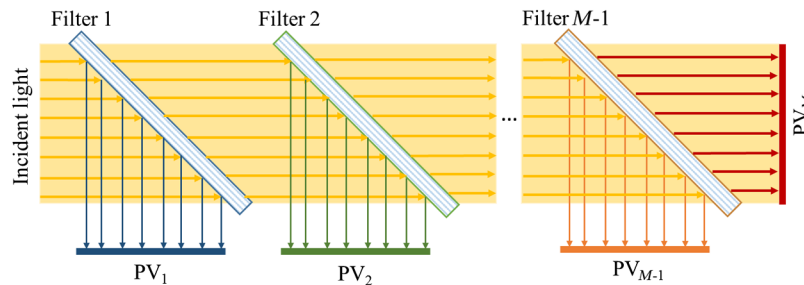


Fig. 1 Spectrum-splitting PV system using reflective type filters.

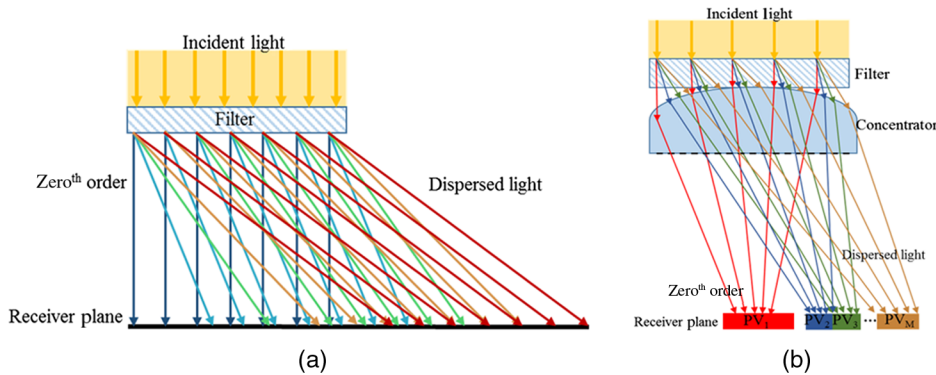


Fig. 2 Dispersive spectrum-splitting PV systems. (a) A single dispersive filter projects the complete spectrum on the receiver plane. Wavelengths overlaps to each other at the receiver plane. (b) A lens is combined with the dispersive filter to focus light and minimize the overlap between spectral bands.

used and is not restricted by current matching effects. Optical spectrum splitting can effectively be achieved with reflective nondispersive and dispersive transmission configurations. In the reflection geometry, one or more reflection bandpass filters are used, which reflect the desired spectral band into a PV cell and transmit the rest into the other PV cell or the next filter (Fig. 1).⁹ The dispersion approach applies a transmission type optics, which consists of either prisms or diffraction gratings to laterally split the incident spectrum at a receiver plane (Fig. 2).⁵⁻⁸ Compared with the reflection approach, the transmission-type dispersive spectrum-splitting arrangement is simpler for systems with more than two junctions, and also lends itself to low-cost mass production methods. However, to achieve a high-efficiency dispersive SSPV system, optical filters that efficiently and accurately send the correct energy photons to the right location at the receiver plane are required.

2.1 Efficiency of SSPV Systems

The spectrum-splitting element in a SSPV system matches the PV cell spectral responsivity with portions of the incident spectrum to achieve higher conversion efficiency. For an SSPV system with N junctions or energy bandgaps, the power conversion efficiency of the k 'th solar cell can be expressed as

$$\eta_k = \frac{1}{P} \int_{-\infty}^{+\infty} E(\lambda) \eta_k^{\text{opt}}(\lambda) \text{SCE}_k(\lambda) d\lambda, \tag{1}$$

where η_k is the filtered power conversion efficiency of the k 'th solar cell, $E(\lambda)$ is the incident power spectrum (PS), P is the total incident power for all wavelengths, $\eta_k^{\text{opt}}(\lambda)$ is the spectral optical efficiency of the optical filter for the k 'th cell, and the $\text{SCE}_k(\lambda)$ is the spectrum conversion efficiency (SCE) of the cell. An accurate expression for $\text{SCE}_k(\lambda)$ can be calculated using the detailed balance method with the incident PS.⁶

The overall power conversion efficiency for such a system can then be calculated with

$$\eta_{\text{sys}} = \sum_{k=1}^N \eta_k. \tag{2}$$

The goal of optimizing an SSPV system is to maximize the optical power conversion efficiency with the incident solar spectral power distribution. This requires that (1) each PV cell in the system either increases the SCE over other cells in regions, where the spectral responsivity overlaps or extends the wavelength range of the solar spectrum that is converted; (2) the optical efficiency of the filter [$\eta_k^{\text{opt}}(\lambda)$] is maximized within its spectral band and minimized elsewhere. These criteria are used in the design of holographic optical filters to optimize the power conversion efficiency of the SSPV system.

2.2 Evaluating Optical Filters

In a spectrum-splitting system, the spectral responsivity of the PV cells and the optical filter function contributes to the overall efficiency of the system. The optical spectral efficiency of an ideal filter for the k 'th PV cell can be expressed as

$$\eta_{k,\text{ideal}}^{\text{opt}}(\lambda) = \begin{cases} 1 & \left(\frac{hc}{E_g^{k-1}} \leq \lambda < \frac{hc}{E_g^k} \right), \\ 0 & \text{Otherwise} \end{cases}, \tag{3}$$

where h is the Planck constant, c is the speed of light, E_g^k is the bandgap energy of the k 'th PV cell, and E_g^{k-1} is the bandgap energy of the $(k - 1)$ 'th PV cell whose bandgap energy is greater than the k 'th PV cell. In actual systems, the filter efficiency is <1 for at least part of the spectral band, and this reduces the conversion efficiency of the SSPV system.

To only evaluate the performance of the optical filters, we assume that the PV cells used in the system absorb all the photons with energy less than their bandgap energy (i.e., EQE = 1). In this case, Eq. (1) can be simplified to

$$\begin{aligned}
 \eta_k &= \frac{1}{P} \int_{-\infty}^{+\infty} E(\lambda) \eta_k^{\text{opt}}(\lambda) \text{SCE}_k(\lambda) d\lambda \\
 &= \frac{1}{P} \int_{-\infty}^{+\infty} Q(\lambda) \left(\frac{hc}{\lambda} \right) \eta_k^{\text{opt}}(\lambda) \frac{\text{EQE}_k(\lambda)}{hc/\lambda} qV_{oc} FF d\lambda \\
 &= \frac{1}{P} \int_{-\infty}^{+\infty} Q(\lambda) \eta_k^{\text{opt}}(\lambda) [\text{EQE}_k(\lambda) qV_{oc} FF] d\lambda \\
 &= C(E_g^k) \int_{\lambda_1}^{\lambda_2} Q(\lambda) \eta_k^{\text{opt}}(\lambda) d\lambda,
 \end{aligned} \tag{4}$$

where $Q(\lambda)$ is the incident spectral photon density; λ_1 and λ_2 are the wavelengths that have photon energies equal to the bandgap energies of the k 'th and $(k-1)$ 'th PV cells; $\text{EQE}_k(\lambda)$ is the external quantum efficiency of the k 'th PV cell, which is equal to 1 when λ is within the $[\lambda_1, \lambda_2]$ range; hc/λ is the photon energy of the photon with wavelength λ ; and q is the electron charge. V_{oc} and FF are the open circuit voltage and fill factor of the PV cell, which can be defined using detailed balance analysis. To simplify the analysis, V_{oc} and FF are assumed to be independent of the wavelength. With these conditions, $C(E_g^k)$ is a constant, which is only related to the bandgap energy of the k 'th PV cell.

To optimize Eq. (4), an optical fill factor (OFF) metric can be used, which is evaluated with a specific illumination spectrum. This metric is defined as the average of weighted optical quantum efficiency over the desired filtering spectral band

$$\text{OFF}_k = \frac{1}{Q_{\lambda_1, \lambda_2}} \int_{\lambda_1}^{\lambda_2} \eta_k^{\text{opt}}(\lambda) \times Q(\lambda) d\lambda, \tag{5}$$

where n_k is the ideal factor of the filtering optics of the k 'th PV cell, and Q_{λ_1, λ_2} is the total number of incident photons within the desired filtering spectral band: $[\lambda_1, \lambda_2]$. The OFF metric compares the number of photons that arrive at the k 'th PV cell surface and are absorbed by the cell with the total number of incident photons within the desired absorption spectral band in which the PV cell obtains the highest SCE in the system. This parameter is useful because the maximum power output of a PV cell is directly proportional to the number of photons that are absorbed (i.e., the number of electric-hole pairs been generated).

However, in a SSPV system, the OFFs of different bandgap cells are not independent of each other. As shown in Fig. 3, a large OFF for filter 1 can lead to a small OFF for filter 2. Therefore, to optimize the optical performance of the overall system, it is necessary to consider a metric, which considers all spectral bands in the system and the contribution of each bandgap. Based on these conditions, the system optical factor (SOF) can be defined as

$$\text{SOF} = \frac{\sum_{k=1}^N \text{OFF}_k \times E_g^k}{\sum_{k=1}^N E_g^k}. \tag{6}$$

This SOF is now used as a figure of merit to optimize the optical filters in spectrum-splitting system.

In a dispersive SSPV system, the loss resulting from the optical elements is usually due to: (1) mismatch between the diffracted spectrum and the desired absorption band of the PV cell,

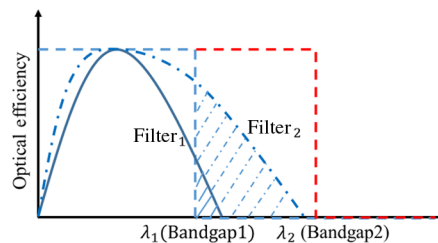


Fig. 3 Trade-off relation of OFFs between bandgaps. Filter 2 has a larger OFF than filter 1 for bandgap1 PV cells. However, it also results a lower OFF than filter 1 for bandgap 2.

Table 1 The optimized sets of bandgaps and corresponding transition wavelengths for 2-, 3-, and 4-junction MJPV system in standard one sun condition.

N	η (%)	E_{g1} (eV)	E_{g2} (eV)	E_{g3} (eV)	E_{g4} (eV)	λ_1 (nm)	λ_2 (nm)	λ_3 (nm)	λ_4 (nm)
2	46.06	1.73	0.94	—	—	717	1319	—	—
3	51.94	2.05	1.4	0.93	—	605	886	1333	—
4	55.91	2.23	1.64	1.13	0.7	556	756	1097	1771

(2) low diffraction efficiency (DE) over the spectral band, and (3) overlap between diffracted spectral bands. Several papers have demonstrated that the losses from (3) can be minimized by concentrating the dispersed spectral bands diffracted by the holographic elements. This can be achieved either using an additional focusing system,⁵⁻⁷ or adding power directly into the diffractive element.⁸ In this research, we only focused on minimizing the loss from (1) and (2) of the holographic spectrum-splitting elements, and assume no loss due to (3).

2.3 Bandgap Combinations

The bandgap combination for the SSPV system is determined based on the requirement to achieve the maximum power conversion efficiency of the system when $\text{OFF}_k = 1$ for all bandgaps. Under these conditions, the detailed balance limit can be computed for an N -junction PV system under AM1.5G spectrum.¹⁴ This method has been used to optimize the bandgaps to predict the efficiency limit for two-, three, and four-junction systems without current matching constraints and are listed in Table 1. In Sec. 3, holographic spectrum-splitting elements are designed for maximum power conversion efficiency with the two- and three-cell combinations listed in Table 1. Both single and cascaded holographic elements are considered in the design and optimization process.

3 Design of Holographic Spectrum-Splitting Elements

Volume holographic elements are good candidates for transmission-type dispersive spectrum-splitting filters. This is because volume holograms are inherently dispersive since it is a diffraction grating and can be designed to diffract a specific spectral band with high DE. In addition, the elements can be mass produced at low cost. DCG is a well-known material for making high-quality volume holograms.¹⁵ This material can provide a wide range in refractive index modulation (0.001 to 0.08) and after sealing has long-term stability properties under solar illumination.¹⁶ Using different deposition techniques, the film thickness can also be varied from 2 to 25 μm to control the initial spectral bandwidth range. Further modification to the shape and width of the diffracted spectral bandwidth can be achieved by varying the film processing method.

In this design, we focused on optimizing DCG holographic spectrum-splitting elements to obtain the most efficient two- and three-junction SSPV systems (Table 1). The optimization process focuses on maximizing the SOF as shown in Eq. (6). For each of the corresponding bandgap combinations shown in Table 1, both single and two-layer cascaded holographic spectrum-splitting elements are designed and optimized. The power conversion efficiencies for the corresponding systems are then calculated using detailed balance method to obtain the limits of SSPV systems using holographic spectrum-splitting elements.

3.1 SSPV System Model

A unit element of the holographic dispersive spectrum-splitting system is shown in Fig. 4. This system consists of a holographic filter placed above a lens array with aspheric lenses to direct different components of the solar spectrum onto the most efficient PV cells. A series of PV cells with different bandgap energies is arranged horizontally at the receiver plane to receive

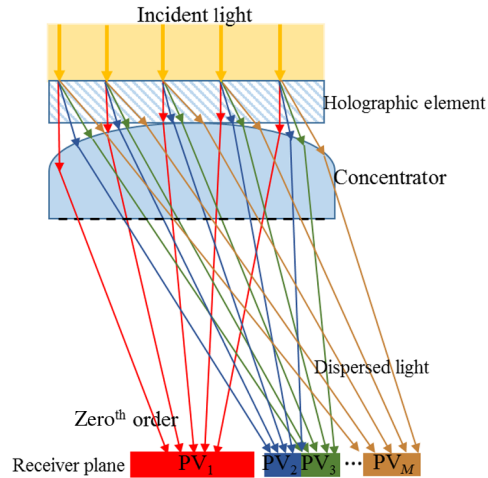


Fig. 4 The structure of a dispersive holographic spectrum-splitting system with a perfect focusing element.

the corresponding spectrum components. The narrow bandgap (NBG) PV cell is located along the axis of the system and the wider bandgap cells are located at a position corresponding to the designed diffraction angle. The hologram is designed to diffract normally incident light, which allows diffuse light entering at larger angles to be passed through the hologram and be converted by the NBG PV cell to increase energy yield.

In this study, we aimed at finding the efficiency limit of a DCG-based holographic SSPV system. A few assumptions are made to simplify the model.

1. The concentrating lens is ideal: no aberrations or residual dispersion by the lens.
2. The concentration ratio is high enough to avoid spectral overlap at the PV cells.
3. PV cells used in the system absorb all photons that exceed the energy bandgap. Detailed balance method is used to calculate the power conversion efficiency of each cells in the system.
4. The holographic spectrum-splitting elements satisfy the conditions for approximate coupled wave analysis.¹⁶

3.2 Modeling Holographic Spectrum Splitter

The holographic gratings using in this study are modeled with Kogelnik's coupled wave analysis.¹⁷ The variables used in optimization include the hologram thickness, refractive index modulation, grating period, peak diffraction wavelength, and diffraction angles. The hologram parameters are consistent with the capability of the DCG material and the design of the holographic SSPV system.

3.2.1 Single-layer spectrum-splitting elements

The single-layer holographic spectrum-splitting elements are designed and optimized using the Kogelnik coupled wave model and the figure of merit defined in Sec. 2.2 for both two- and three-junction SSPV systems. The design considerations include: (1) the diffraction angle and wavelength to specify the surface grating period (x -component of the grating vector: \vec{K}) that determine the ray trajectories and (2) the wavelength that optimizes the DE to maximize the conversion efficiency of the PV cells. This wavelength is Bragg matched to the volume grating vector by determining z -component of the \vec{K} vector. (3) The spectral DE and bandwidth, which are determined by the hologram material properties including the index modulation, film thickness, and \vec{K} vector.

The first step to designing a transmission volume hologram is to determine the grating periods in both surface and depth directions. The holographic filters are designed for normal incident

Table 2 Search range and step increment of the parameters using in hologram optimization.

	Two junction (1.73 and 0.94 eV)		Three junction (2.05, 1.4, and 0.93 eV)	
	Range (min–max)	Step separation	Range (min–max)	Step separation
λ_{Bragg} (nm)	300 to 717	5	300 to 886	5
θ_{Bragg} (deg)	10 to 25	1	10 to 35	1
Grating thickness (μm)	1 to 25	1	1 to 25	1
Index modulation	0 to 0.1	0.002	0 to 0.1	0.002

illumination. To obtain high DE at the desired peak efficiency wavelength with a certain diffraction angle, both the grating equation and Bragg condition¹⁶ must be satisfied. In this case, the grating period components along the surface direction, Λ_x , and depth direction, Λ_z , can then be determined according to

$$\Lambda_x = \frac{\lambda_{\text{Bragg}}}{n \sin(\theta_{\text{Bragg}})}, \quad (7)$$

$$\Lambda_z = \frac{\lambda_{\text{Bragg}}}{n[1 - \cos(\theta_{\text{Bragg}})]}, \quad (8)$$

where λ_{Bragg} is the Bragg-matched wavelength, n is the average refractive index of the hologram material, and θ_{Bragg} is the diffraction angle of λ_{Bragg} .

The next step is to use the Kogelnik approximate coupled wave analysis to calculate the spectral DE of the volume transmission phase grating

$$\eta(\lambda) = \frac{\sin^2[\nu(\lambda)^2 + \xi(\lambda)^2]^{1/2}}{[1 + \xi(\lambda)^2/\nu(\lambda)^2]}, \quad (9)$$

where $\eta(\lambda)$ is the spectral DE, $\nu(\lambda) = \frac{\pi n_1 h}{\lambda c_r(\lambda) c_s(\lambda)}$ is the grating strength parameter, $\xi(\lambda)$ is a parameter defined as $\xi(\lambda) = \frac{\vartheta(\lambda)h}{2c_s(\lambda)}$, n_1 is the refractive index modulation, h is the thickness of the grating, c_r and c_s are the cosine values of the incident and diffracted beams, and $\vartheta(\lambda)$ is the detuning parameter, respectively.

A final design condition for the holographic elements is to satisfy the volume quality or Q factor for the grating defined by $Q = \frac{2\pi\lambda_{\text{peak}}h}{n\Lambda^2} \geq 10$. Having the hologram parameters satisfy this relation ensures that the volume condition is satisfied and that a single high-efficiency diffraction order will result.

Based on this model, the spectral optical properties of a single-layer spectrum-splitting hologram can be modified by setting the: (1) Bragg matched wavelength, (2) diffraction angle of λ_{Bragg} , (3) grating thickness, and (4) refractive index modulation. To optimize a hologram for specific SSPV system, a search algorithm is used that searches through the possible values of these four parameters to obtain the highest SOF for the desired two- and three-junction SSPV system. Table 2 shows the searching range and step increment for each parameter, which are varied through the values for practical DCG emulsions.

3.2.2 Two-layer cascaded spectrum-splitting element

The two-layer cascaded spectrum-splitting element consists of two stacked-volume holograms as shown in Fig. 5. It is easier to achieve a “near ideal” filter function with the cascaded configuration due to a larger set of hologram design parameters. In general, it is possible to achieve both a broader spectral bandwidth and sharper transition edge for the resulting filter.

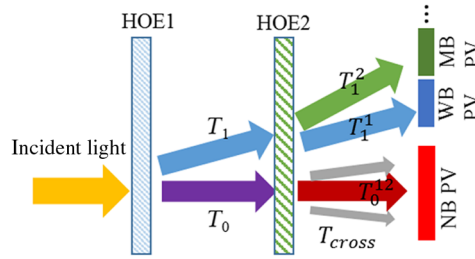


Fig. 5 Input and output orders and PV cell locations for a two-layer cascaded SSPV system.

However, the holograms must be designed to minimize cross-coupling effects. As shown in Fig. 5, if the same diffraction angles and wavelengths are used for both gratings, light diffracted by HOE₁ into the first diffracted order T_1 will be coupled back into the zero order (T_0^{12}). If cross coupling is not minimized, the diffracted spectral components will not reach the PV cell for maximum conversion efficiency.

To optimize a two-layer cascaded holographic spectrum splitter, the top and the bottom holograms are optimized by searching through the parameters shown in Table 2 using single-hologram model described in Sec. 3.2.1. At each iteration, the spectral diffraction efficiencies of HOE₁ and HOE₂ [$\eta_1(\lambda)$ and $\eta_2(\lambda)$], and the cross-coupling efficiency [$\eta_{cross}(\lambda)$] for T_1 passing through HOE₂ are calculated. The overall filtering efficiency for this grating can be expressed as

$$\eta(\lambda) = \eta_1(\lambda) \times [1 - \eta_{recouple}(\lambda)] + [1 - \eta_1(\lambda)] \times \eta_2(\lambda). \quad (10)$$

This efficiency is then applied to two- and three-junction SSPV system configuration to calculate the SOF.

3.3 Optimization and Modeling Results

Based on the approximate coupled wave model and the optimization methods described in Sec. 3.2, programs are created and run to find the optimized holographic optical elements

Table 3 The optimized parameters for the single HOEs and the cascaded filters using in the optimized two- and three-junction spectrum-splitting PV system.

Optimized parameters	Two junction (1.73 and 0.94 eV)			Three junction (2.05, 1.4, and 0.93 eV)		
	Single HOE	HOEs in cascaded filter		Single HOE	HOEs in cascaded filter	
		Top (1)	Bottom (2)		Top (1)	Bottom (2)
OFF (WBF)	0.8236	0.894		0.8431	0.8582	
OFF (MBF)	—	—		0.5813	0.756	
OFF (NBF)	0.8593	0.8981		0.947	0.9313	
SOF	0.8361	0.8954		0.7941	0.8411	
Bragg matched WL (nm)	525	500	500	565	535	805
Diffraction angle (deg)	21	21	14	23	18	31
Δx (μm)	0.943	0.943	1.3508	0.943	1.1292	1.012
Δz (μm)	5.0063	5.2746	11.002	4.6247	7.1134	3.5836
Grating thickness (μm)	6	16	12	6	8	14
Index modulation	0.06	0.09	0.02	0.064	0.042	0.02
Q factor	10.0404	87.0526	41.4007	11.3906	10.5994	48.7424

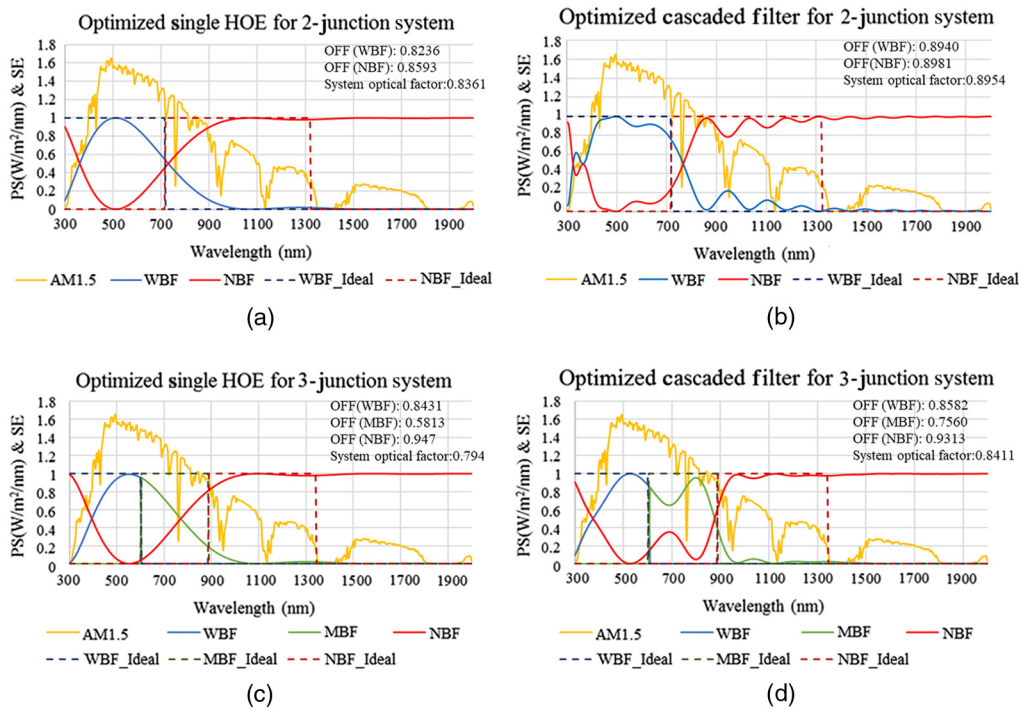


Fig. 6 The SOFEs of all PV bandgaps using in optimized two- and three-junction SSPV systems along with the AM1.5 illumination PS. (a) and (b) The SOFEs of the optimized two-junction systems with using single HOE and cascaded filter. (c) and (d) The SOFEs of the optimized three-junction systems with using single HOE and cascaded filter. The red, blue, and green curves are for the system filtering properties of the wide bandgap (WBF), the NBF, and the middle bandgap (MBF).

(HOEs) for the two- and three-junction SSPV systems that are described in Sec. 3.1. The optimized parameters for the HOEs are found for the best bandgap combinations (1.73 and 0.94 eV for two junction; 2.05, 1.4, and 0.93 eV for three junction). These parameters are summarized in Table 3. The results show that the optimized SOF for the two-junction SSPV system reaches 0.836 with single HOE and 0.895 with two-layer cascaded HOE, and for the three-junction system reaches 0.7941 with single HOE, and 0.8411 with the two-layer cascaded filter.

The spectral optical filtering efficiencies (SOFEs) for the optimized two- and three-junction SSPV systems and AM1.5 illumination are plotted in Fig. 6.

The resulting filtering properties were then used to compute the power conversion efficiencies for the different configurations using the detailed balance method.⁴ The improvement over best bandgap (IoBB) is also calculated for each system as a metric for system performance.⁵ For comparison, the efficiencies of tandem MJ PV cells with the same bandgap combinations are

Table 4 The power conversion efficiencies and IoBBs for the optimized two-junction SSCPV systems, tandem PV and ideal condition at AM1.5 solar irradiance.

	Single BG (%)	Two junction (1.73 and 0.94 eV)			
		Single HOE (SS) (%)	Cascaded filter (SS) (%)	Tandem (%)	Ideal (%)
WBF (1.73 eV)	28.77	23.61	25.67	28.74	28.74
NBF (0.94 eV)	30.9	17.36	16.89	12.68	17.32
System power efficiency		40.97	42.56	41.42	46.06
IoBB		32.59	37.73	34.05	49.06

Table 5 The power conversion efficiencies and IoBB for the optimized three-junction SSPV systems, tandem PV, and ideal condition at AM1.5 solar irradiance.

	Three Junction (2.05, 1.4, and 0.93 eV)				
	Single BG (%)	Single HOE (SS) (%)	Cascaded filter (SS) (%)	Tandem (%)	Ideal (%)
WBF (2.05 eV)	22.1	18.06	18.97	21.56	21.56
MBF (1.4 eV)	33.24	11.33	14.88	13.26	19.67
NBG (0.93 eV)	30.7	16.38	14.56	7.5	10.68
System power efficiency		45.77	48.41	42.32	51.91
IoBB		49.09	54.43	27.3	56.17

calculated including the restriction due to current constraints. The results are summarized in Tables 4 and 5 for the two- and three-junction bandgap systems.

With AM1.5 illumination, the simulation results show that the holographic SSPV systems described in this paper have the potential to reach a maximum power conversion efficiency of 42.56% using a DCG holographic filter in the two-junction system, and 48.41% for the three-junction system. The results also show an IoBB of a 37.73% for the two bandgaps and 54.43% for the three bandgap SSPV systems. In addition, the loss due to nonideal DCG filter spectrum splitting is 7.60% for the two bandgaps and 6.74% for the three bandgap SSPV systems.

4 Fabrication of Holographic Spectrum Splitter

To prove the concept, the cascaded holographic grating optimized for the three-junction system was fabricated using DCG films prepared in our lab. The top grating (grating A) and the bottom grating (grating B) were recorded and processed individually, and then sealed with an index matched optical cement to form the desired cascaded filter. The prototyped cascaded grating was then tested and compared with the simulation results.

4.1 Dichromate Gelatin Grating Modeling

As mentioned before, DCG holograms benefits from high refractive index modulation, low scattering, low absorption, and excellent long-term stability properties. However, to develop a high-quality DCG grating with parameters that match the design, an accurate grating model that includes swelling that occurs during the wet development process (described in Sec. 4.2) is required.

Rigorous coupled wave analysis (RCWA)¹⁷ can accurately model grating modulation with a nonuniform profile. Both the average swelling and chirp of the grating period are included as a function of depth. For a planner grating recorded in DCG, the refractive index profile is approximated as

$$n(x, z) = n_{\text{avg}} + n_1 \sin \left\{ \left(\frac{2\pi}{\Lambda_x} x \right) + \left[\frac{2\pi}{\Lambda(z) h} z \right] \right\}, \quad (11)$$

$$\Lambda(z) = \Lambda_z(1 + S) \exp(C * z), \quad (12)$$

where z is the distance from the interface of hologram and substrate, x is the distance from one of the grating edges on the surface direction. $n(x, z)$ is the index value at location of (x, z) , n_{avg} is the average refractive index of DCG, n_1 is the refractive index modulation, Λ_x and Λ_z are the corresponding recorded grating periods in x and z directions, and h is the thickness of the hologram. S and C are the average swelling and chirping coefficients. In this model, the grating

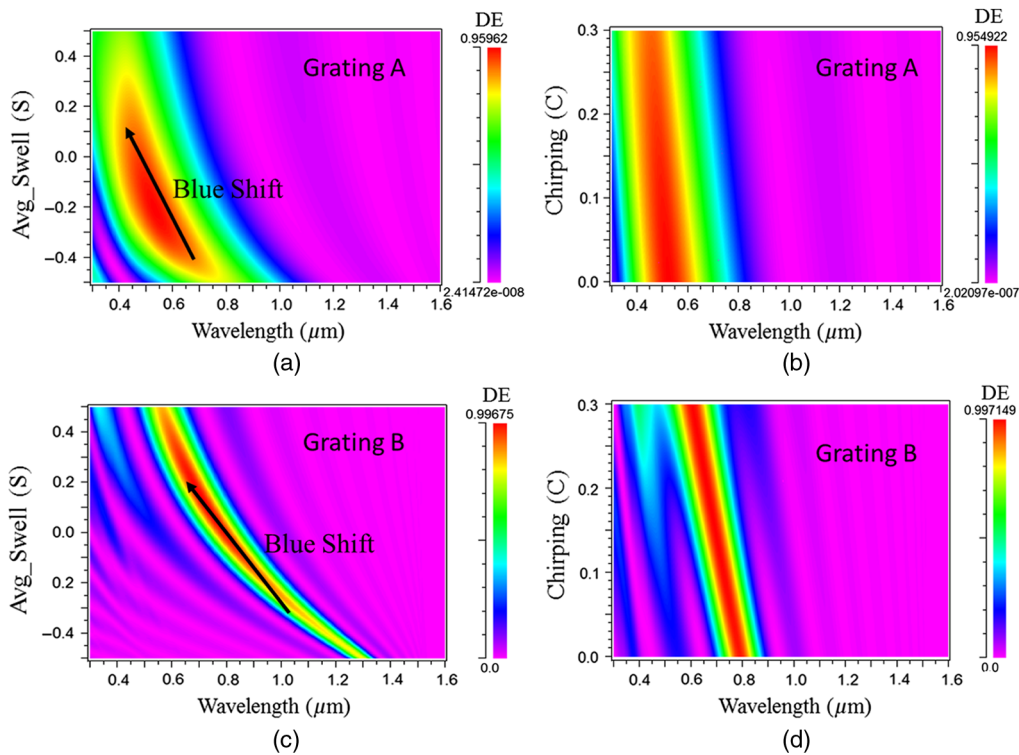


Fig. 7 The spectral diffraction efficiencies as a function of average swelling (S) for the optimized (a) grating A and (c) grating B, and as a function of chirping coefficient (C) for the optimized (b) grating A and (d) grating B.

period in the x -direction remains the same; however, the z -period changes compared with the interference profile recorded during hologram construction.

An Rsoft¹⁸ RCWA simulator was used to compute the DE with the index and period functions given in Eqs. (11) and (12). Figure 7 shows the spectral diffraction efficiencies as a function of S and C for the optimized gratings (A and B) of three-junction system designed in Table 3. The simulation indicates that the average swelling of a transmission grating results in a strong blue shift of the Bragg matched wavelength, and the grating chirp results in a slight blue shift and only a small improvement in spectral bandwidth. Therefore, only controlling the average swelling was emphasized in the DCG development process.

4.2 Fabrication Process

DCG films can be made with various coating techniques. In our lab, the sensitized gelatin mixture was mold coated onto a glass substrate. This mixture was formed with water, gelatin power, and ammonium dichromate (AD) with a respective weight ratio of 50:6:1. The temperature of this solution is maintained at 45°C before the coating process. The mold was made with single layer of spacing tape taped around the perimeter of a clean glass substrate. One to two drops of RainX were then rubbed onto the glass surface and the tapes, to allow the gelled DCG easily removed from the mold. About 3.5 ml of the sensitized gelatin mixture was then dropped onto a cleaned glass substrate, and the mold was placed above the mixture to form it into a thin layer. Pressures are also applied on the sides of the mold. After 45 min gelling in a 10°C envelopment, the mold was removed from the substrate. The DCG-coated substrates were then placed in a fume hood under room temperature and low relative humidity for a 12-h drying process. This process can yield a DCG film with thickness between 8 and 22 μm depending on the spacing tape thickness (1 to 8 mils). The average refractive index of this film was found to be 1.53 with the Brewster angle method.

To form the designed holograms, the DCG film was exposed using a collimated beam from 532-nm DPSS laser as shown in Fig. 8. The construction angles θ_1 and θ_2 for each grating are

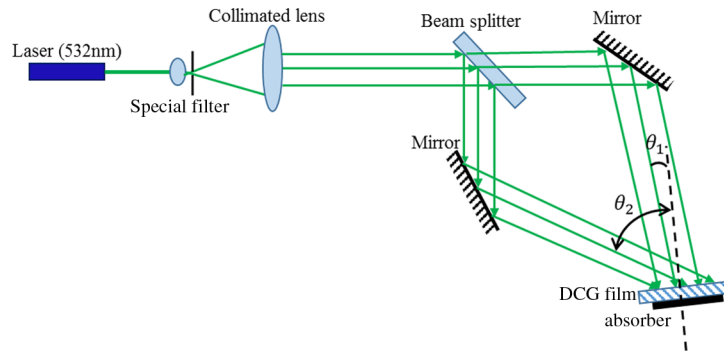


Fig. 8 The exposure geometry for recording holographic filters.

Table 6 The experimental parameters for recording gratings A and B.

	Laser wavelength (nm)	θ_1 (deg)	θ_2 (deg)	Beam ratio	Visibility	Exposure energy (mJ/cm ²)
Grating A	532	5.8	34.9	6:07	0.997	1740.05
Grating B	532	17.01	52.95	5:07	0.91	1002.72

precalculated based on its peak diffraction wavelength, diffraction angle, swelling effects, and the recording wavelength. Under the fixed AD/gelatin ratio, the refractive index modulation of a DCG hologram is determined by the fringe visibility and the total exposure energy on the DCG film. A series of experiments were made to find the desired exposure energy. Table 6 summarized all the parameters for gratings A and B during exposure process. For both recording, the uncoated side of the DCG substrate was index matched with microscope immersion oil ($n = 1.52$) to an optical absorber ($OD = 6.0$) to minimize the parasitic gratings formed by the interference pattern due to the Fresnel reflections of film surfaces.

The typical development process for DCG hologram usually includes a fixing process, a chemical hardening process, a rinse process, a dehydration process, and a thermal drying and hardening process. To keep the same level of average swelling, minimize the chirping effect, and increase the repeatability of the fabrication, a cold dehydration process was used to develop the gratings. The finalized development procedure and the time intervals are shown in Table 7.

Once one of the gratings is developed, it can be stored in a dry box ($RH < 10\%$) for a long periods of time without degradation of its optical properties. After gratings, A and B were fabricated and tested, they were sealed with DCG side face to face using an index matched optical glue.

Table 7 DCG cold development procedure.

1	Fix plate with Kodak fixer A and B at room temperature (25°C)	120 s
2	Rinse in flowing water at room temperature (25°C)	60 s
3	Dehydrate with 50% isopropanol at 25°C	45 s
4	Dehydrate with 75% isopropanol at 25°C	45 s
5	Dehydrate with 99% isopropanol at 25°C	60 s
6	Dry with air gun to remove any remaining isopropanol	5 s
7	Bake in oven at 65°C	15 min

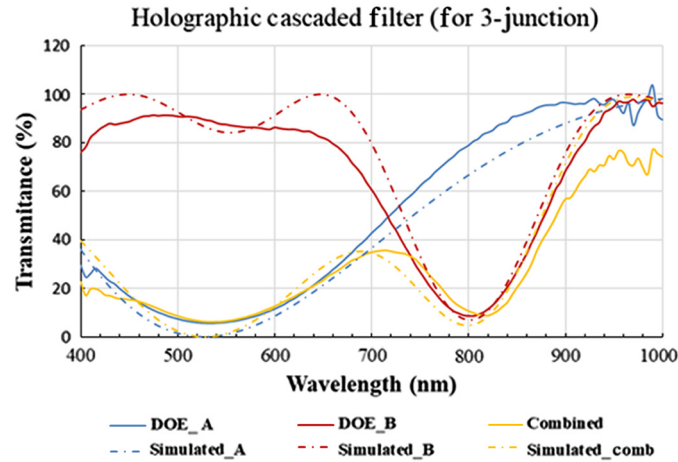


Fig. 9 The measured (solid line) and the simulated (dash line) transmittances of the optimized holographic filters (gratings A, B, and cascaded grating) designed for the three-junction SSPV system.

4.3 Experimental Performance

The diffraction efficiencies of the fabricated holograms (gratings A, B, and the cascaded grating) are obtained by measuring the transmittance spectra of a normal incident broadband source. The spectral transmittance is defined as the transmitted spectral flux of the hologram over that of an uncoated substrate under normal incident angle. The transmittances of the prototype holographic filters and the simulated filters with RCWA model are compared in Fig. 9. The result indicates that the diffraction property of the prototype gratings A and B both match the designed gratings very well.

The thickness of each holograms was measured with a dial indicator with resolution of $0.5 \mu\text{m}$; the diffraction angle was measured using single wavelength lasers (532 nm for grating A and 790 nm for grating B); and the OFFs and OSF are both calculated based on the measured spectral DE. These measurement results for the fabricated holographic grating are summarized and compared with the designed gratings in Table 8. The results show that the prototype grating obtains a high SOF of 0.8297 that results a 46.93% of power conversion efficiency for the three-junction SSPV system.

Table 8 Parameters for prototype gratings compared with the design.

Gratings	Measurement of prototype		Designed parameters	
	A	B	A	B
OFF (WBF)	0.8408		0.8582	
OFF (MBF)	0.755		0.756	
OFF (NBF)	0.9118		0.9313	
SOF	0.8297		0.8411	
Bragg matched WL (nm)	535	805	535	805
Diffraction angle (deg)	18 (at 532 nm)	31(at 790 nm)	18 (at 532 nm)	31 (at 790 nm)
Grating thickness (μm)	10	16	6	14
Resulting SS efficiency (%)	46.93		48.41	
Resulting loBB (%)	41.19		54.43	

5 Conclusions

In this paper, a typical holographic dispersive spectrum-splitting PV system with ideal concentration optics was demonstrated. The design can significantly improve the system power conversion efficiency of multiple bandgap PV systems with well-designed holographic filters. A systematic method for optimizing volume holographic elements for spectrum-splitting systems was described. Single and cascaded holographic filters were modeled with approximate coupled wave analysis. A search algorithm evaluating hologram parameters was developed to optimize both single layer and two-layer cascaded holographic spectrum-splitting elements with different bandgap combinations of two- and three-junction SSCPV system illuminated with an AM1.5 solar spectrum. The variables that were searched in the optimization were limited to the range available for DCG materials. The system power efficiencies were calculated with optimized filters using a detailed balance method. The simulation results show that under AM1.5 illumination, the holographic SSPV systems can reach a maximum limit of 42.56% and 48.41% of power conversion efficiency for two- and three-junction combination using two-layer cascaded holographic spectrum-splitting elements. An IoBB of 37.73% (two-junction) and a 54.43% (three junction) was obtained for the HSSPV systems. Finally, a fabrication process is described to prototype the cascaded DCG holographic filter designed for the three-junction SSCPV system. The prototyped grating obtains similar optical properties as the design with a SOF of 0.8065 that can result a 46.93% of power conversion efficiency, and 41.19% of IoBB for the two-junction SSCPV system.

Acknowledgments

The authors wish to acknowledge support from the NSF/DOE ERC cooperative agreement No. EEC-1041895, NSF Grant No. ECCS-1405619.

References

1. A. Polman and H. A. Atwater, "Photonic design principles for ultrahigh-efficiency photovoltaics," *Nat. Mater.* **11**(3), 174–177 (2012).
2. A. Martí and A. Luque, *Next Generation Photovoltaics High Efficiency Through Full Spectrum Utilization*, pp. 108–119, Institute of Physics Publishing, Bristol and Philadelphia (2004).
3. R. McConnell, "Concentrator photovoltaic technologies: review market prospects," *Refocus* **6**, 35–39 (2005).
4. W. Shockley and H. J. Queisser, "Detailed balance limit of efficiency of p-n junction solar cells," *J. Appl. Phys.* **32**(3), 510–519 (1961).
5. J. M. Russo et al., "Grating-over-lens concentrating photovoltaic spectrum splitting systems with volume holographic optical elements," *Proc. SPIE* **8821**, 882106 (2013).
6. Y. Wu and R. K. Kostuk, "Two-junction holographic spectrum-splitting micro concentrating photovoltaic system," *J. Photonics Energy* **7**(1), 017001 (2017).
7. Y. Wu et al., "Three junction holographic micro-scale PV system," *Proc. SPIE* **9937**, 99370M (2016).
8. S. D. Vorndran et al., "Off-axis holographic lens spectrum-splitting photovoltaic system for direct and diffuse solar energy conversion," *Appl. Opt.* **55**, 7522–7529 (2016).
9. J. D. McCambridge et al., "Compact spectrum splitting photovoltaic module with high efficiency," *Prog. Photovoltaics Res. Appl.* **19**(3), 352–360 (2011).
10. C. Maragliano, M. Chiesa, and M. Stefancich, "Point-focus spectral splitting solar concentrator for multiple cells concentrating photovoltaic system," *J. Opt.* **17**(10), 105901 (2015).
11. L. Z. Broderick et al., "Design for energy: modeling of spectrum, temperature and device structure dependences of solar cell energy production," *Sol. Energy Mater. Sol. Cells* **136**, 48–63 (2015).
12. A. Barnett et al., "Very high efficiency solar cell modules," *Prog. Photovoltaics Res. Appl.* **17**(1), 75–83 (2009).

13. G. B. Ingersoll and J. R. Leger, "Optimization of multi-grating volume holographic spectrum splitters for photovoltaic applications," *Appl. Opt.* **55**, 5399–5407 (2016).
14. S. P. Bremner, M. Y. Levy, and C. B. Honsberg, "Analysis of tandem solar cell efficiencies under AM1.5G spectrum using a rapid flux calculation method," *Prog. Photovoltaics Res. Appl.* **16**, 225–233 (2008).
15. B. J. Chang and C. D. Leonard, "Dichromated gelatin for the fabrication of holographic optical elements," *Appl. Opt.* **18**(14), 2407–2417 (1979).
16. H. Kogelnik, "Coupled wave theory for thick hologram gratings," *Bell Syst. Tech. J.* **48**(9), 2909–2947 (1969).
17. M. G. Moharam and T. K. Gaylord, "Rigorous coupled-wave analysis of planar-grating diffraction," *J. Opt. Soc. Am.* **71**, 811–818 (1981).
18. "Rsoft™," Synopsys, <https://www.synopsys.com/optical-solutions/rsoft.html> (06 October 2017).

Yuechen Wu received his bachelor of science degree in electrical and computer science engineering at the University of Toledo in 2012. Currently, he is pursuing his PhD in electrical and computer engineering and working at the Photonic System Laboratory at the University of Arizona. His research interests include diffractive optics, optical engineering, micro-optics, and solar energy.

Benjamin Chrysler received his bachelor's degree in electrical engineering from Colorado State University and his Master's degree in electrical engineering at the University of Arizona. He is a PhD student in optical sciences at the University of Arizona. His research interests are in optical system design with a focus on holographic optical elements and photovoltaic systems. He is a recipient of the National Science Foundation Graduate Student Fellowship.

Raymond K. Kostuk has a joint professor position at UA's ECE Department and the College of Optical Sciences. He received his PhD in electrical engineering from Stanford University. His primary area of expertise is in holographic concepts, materials, and applications, with over 30 years of experience in that area. He is a fellow of the Optical Society of America and SPIE.